CASI

FINAL

REPORT

NASA Grant No.: NAG1-1883

Computation of Anisotropic Bi-Material Interfacial Fracture Parameters & Delamination Creteria

Center for Aerospace Research & Education
7704 Boelter Hall
School of Engineering & Applied Science
UCLA, Los Angeles, CA. 90095-1600, USA

Feb. 1998

TABLE OF CONTENTS

Computation of Anisotropic Bi-Material Interfacial Fracture Parameters & Delamination Creteria

W-T. Chow, L. Wang and S.N. Atluri

Feb. 1998

Center for Aerospace Research & Education

7704 Boelter Hall

School of Engineering & Applied Science

UCLA, Los Angeles, CA. 90095-1600, USA

This report documents the recent developments in methodologies for the evaluation of the integrity and durability of composite structures, including i) the establishment of a stress-intensity-factor based fracture criterion for bimaterial interfacial cracks in anisotropic materials (see Sec. 2); ii) the development of a virtual crack closure integral method for the evaluation of the mixed-mode stress intensity factors for a bimaterial interfacial crack (see Sec. 3). Analytical and numerical results show that the proposed fracture criterion is a better fracture criterion than the total energy release rate criterion in the characterization of the bimaterial interfacial cracks. The proposed virtual crack closure integral method is an efficient and accurate numerical method for the evaluation of mixed-mode stress intensity factors.

1 Introduction

Laminated composites made of graphite epoxy have a higher stiffness modulus than aluminum, as well as other prefered material properties, which make them highly attractive. As a result, their application have been steadily increasing in the past decades. Among the various failure mechanisms for laminated composites, the propagation of a delamination crack is often the leading cause of global failure for a structural component. Therefore, the potential disbonding is one of the critical problems in the evaluation of the integrity of composite structures. This research is to enhance the capability to predict the strength of structural components made of composite materials.

The prediction of the onset of propagation of a delamination crack in a laminated composite was often based on the total energy release rate of the delamination crack. However, various recent experiments have pointed out that the critical energy release rate of a delamination crack is dependent on the combination of individual modes of failure; mode I (opening), mode II (shearing),

and mode III (tearing). For example, the critical energy release rate for a mode I fracture is an order of magnitude less than the critical energy release rate for a mode III fracture in a T300-5208 unidirectional laminate. Hence, the critical total energy release rate for any two delamination cracks would be quite different unless the ratio of mixity of the fracture modes is similar. This indicates that total enegy release rate is not a good candidate as a fracture criterion for a mixed mode fracture.

Some researchers have suggested the use of the components of mixed-mode energy release rates as the fracture criteria for a delamination crack between two dissimilar lamina. However, numerical (finite element) results [Sun and Jih (1987) and O'Brien (1982)] indicates that the individual components, in mode I and mode II, of the energy release rates for an interfacial crack are strongly dependent on the mesh refinement of the finite element model. Raju et al. (1988) has shown mathematically that the mixed-mode energy release rates of an interfacial crack does not converge upon mesh refinement, using crack-closure integrals in the context of an analysis based on finite element method. In addition, Chow and Atluri (1995) have shown that the three individual mixed-mode energy release rates, (G_I, G_{II}, G_{III}), are insufficient to characterize the stresses and displacements near the interfacial crack tip. Coupled mixed-mode energy release rates, (G_{II-III}, G_{I-III}, G_{I-II}) are required to fully describe the asymptotic stresses and displacements near an interfacial crack tip. Therefore, it is cumbsome to use components of energy release rates for fracture criteria.

However, the mixed-mode stress intensity factors of an interfacial crack are not dependent on the numerical model, unlike the mixed-mode energy release rate components. In the area of interfacial fracture mechanics for isotropic bimaterials, the mixed-mode stress intensity factors are preferred by many researchers as the fracture parameters to define the toughness function of an interfacial crack. The mixed-mode stress intensity factors for an interfacial crack between dissimilar isotropic media were first defined by Williams (1959), and Rice and Sih (1965). They have found that the stress oscillates and the crack surface overlaps near the interfacial crack tip in a linear elastic fracture analysis. However, this solution can be justified [Rice (1988)] in engineering sense when the nonlinear material behavior and crack surface contact zone exists only in a small scale at the crack tip.

The acceptance of stress intensity factors for laminated composites has been slow, until recently a clear mathematical definition of stress intensity factors for an interfacial crack in an anisotropic bimaterial continuum has been established [see Wu (1989); Qu and Li (1991) and Qu and Bassani (1993)]. This definition of stress intensity factors reduces to the classical definition of stress intensity factors when the bimaterial continuum degenerates to a homogeneous one. This report documents the development of a fracture criterion based on this definition of stress intensity factors and numerical methods for its evaluation.

2 A Stress-Intensity-Factor Based Fracture Criterion

2.1 Crack tip solution for a bimaterial interfacial crack

Consider a two dimensional deformation in an anistropic material, in which the displacements depend on the Cartesian coordinates, x_1 and x_2 only. The stress σ_{ij} and strain ε_{kl} satisfy the following constitute relation.

$$\sigma_{ij} = \sum_{k=1}^{3}\sum_{l=1}^{3} C_{ijkl}\varepsilon_{kl} \tag{1}$$

Three distinct complex eigenvalues p_j (with positive imaginary parts), and two eigenmatrices $\mathbf{A}_{3\times3}$ and $\mathbf{B}_{3x3}$ can be defined from the modulus' C_{ijkl} using Eq. 2.

$$\begin{bmatrix} -\mathbf{T}^{-1}\mathbf{R}^T & \mathbf{T}^{-1} \\ \mathbf{R}\mathbf{T}^{-1}\mathbf{R}^T - \mathbf{Q} & -\mathbf{R}\mathbf{T}^{-1} \end{bmatrix} \begin{bmatrix} \mathbf{A} \\ \mathbf{B} \end{bmatrix} = \begin{bmatrix} \mathbf{A} \\ \mathbf{B} \end{bmatrix} \begin{bmatrix} p_1 & 0 & 0 \\ 0 & p_2 & 0 \\ 0 & 0 & p_3 \end{bmatrix} \tag{2}$$

where

$$Q_{ik} = C_{i1k1} \qquad R_{ik} = C_{i1k2} \qquad T_{ik} = C_{i2k2} \tag{3}$$

The eigenmatrices **A** and **B** can be normalized so that

$$\begin{bmatrix} \mathbf{A}^T & \mathbf{B}^T \end{bmatrix} \begin{bmatrix} 0 & \mathbf{I}_{3\times3} \\ \mathbf{I}_{3\times3} & 0 \end{bmatrix} \begin{bmatrix} \mathbf{A} \\ \mathbf{B} \end{bmatrix} = \mathbf{I}_{6\times6} \tag{4}$$

where **I** is the identity matrix.

Two real matrices, **S** and **L**, can then be defined by the normalized eigenmatrices, **A** and **B**, as

$$\mathbf{L} = -2i\mathbf{B}\mathbf{B}^T \qquad \mathbf{S} = i\left(2\mathbf{A}\mathbf{B}^T - \mathbf{I}\right) \tag{5}$$

In an anisotropic bimaterial medium of material (1) and material (2), a bimaterial matrix $\widehat{\boldsymbol{\beta}}$ can be defined as

$$\widehat{\boldsymbol{\beta}} = \left(\mathbf{L}^{(1)^{-1}} + \mathbf{L}^{(2)^{-1}}\right)\left(\mathbf{S}^{(1)}\mathbf{L}^{(1)^{-1}} - \mathbf{S}^{(2)}\mathbf{L}^{(2)^{-1}}\right) \tag{6}$$

where superscripts (1) and (2) signify material #1 and material #2, respectively.

Using the complex variables, z_j (j=1,2,3), defined by

$$z_j = x_1 + p_j x_2 \tag{7}$$

one can express a displacement field (u_i) and its assoicated stress field (σ_{ji}) in the anisotropic medium using three analytic complex functions, $f_1(z_1), f_2(z_2), f_3(z_3)$.

$$u_i = 2\mathrm{Re}\left[\sum_{j=1}^{3} A_{ij} \int f_j(z_j)\right] \tag{8}$$

$$\sigma_{1i} = -2\mathrm{Re}\left[\sum_{j=1}^{3} B_{ij} p_j f_j'(z_j)\right] \tag{9}$$

$$\sigma_{2i} = 2\mathrm{Re}\left[\sum_{j=1}^{3} B_{ij} f_j'(z_j)\right] \tag{10}$$

Consider a semi-infinite and traction-free crack between two anisotropic media of material (1) and material (2) [see Beom and Atluri (1994) for more details]. The three complex functions $f\prime_j^{(m)}(z_j)$, for material #1 and #2 are:

$$f\prime_j^{(1)^{(m)}}(z_j) = \frac{1}{2\sqrt{2\pi z_j}} \hat{\mathbf{e}}_j^T \mathbf{B}^{(1)^{-1}} \left(\mathbf{I} + i\hat{\boldsymbol{\beta}}\right) \mathbf{Y}(z_j^{i\varepsilon})\, \hat{\mathbf{e}}_m (m = 1,2,3) \tag{11}$$

$$f\prime_j^{(2)^{(m)}}(z_j) = \frac{1}{2\sqrt{2\pi z_j}} \hat{\mathbf{e}}_j^T \mathbf{B}^{(2)^{-1}} \left(\mathbf{I} - i\hat{\boldsymbol{\beta}}\right) \mathbf{Y}(z_j^{i\varepsilon})\, \hat{\mathbf{e}}_m \tag{12}$$

where

$$\mathbf{Y}(z_j^{i\varepsilon}) = \mathbf{I} + \frac{i}{2\beta}\left\{ z_j^{i\varepsilon} - z_j^{-i\varepsilon} \right\} \hat{\boldsymbol{\beta}} + \frac{1}{\beta^2}\left[1 - \frac{1}{2}\left\{ z_j^{i\varepsilon} + z_j^{-i\varepsilon} \right\}\right] \hat{\boldsymbol{\beta}}^2 \tag{13}$$

$$\beta = \left\{ -\frac{1}{2} tr\left(\hat{\boldsymbol{\beta}}^2\right) \right\}^{\frac{1}{2}} \tag{14}$$

$$\varepsilon = \frac{1}{2}\pi \ln\left(\frac{1+\beta}{1-\beta}\right) \tag{15}$$

and $\hat{\mathbf{e}}_j$ (j=1,2) are the normalized base vectors. Note the difference between the matrix $\hat{\boldsymbol{\beta}}$ and the scalar variable β.

When the analytic functions, $f_j'^{(m)}(z_j)$, are substituted into Eq. 8-10, one obtains the crack tip stress field and displacement field.

The stress along the interface is

$$\boldsymbol{\tau}(x_1) = \frac{1}{\sqrt{2\pi x_1}} \mathbf{Y}\left(x_1^{i\varepsilon}\right) \mathbf{k} \tag{16}$$

where $\boldsymbol{\tau}$ is $\{\, \sigma_{12}, \sigma_{22}, \sigma_{23} \,\}^T$; and $\mathbf{k} \equiv \{K_{II}, K_I, K_{III}\}^T$ is the vector of stress intensity factors.

2.2 *Equivalent stress intensity factors for the characterization of mixed-mode singular stress fields*

Consider an interfacial crack between two laminae, $[\theta, \alpha]$, where the ply angles of the upper and lower plies are θ and α respectively. For a crack in a homogeneous material, in which θ is equal to α, the singular stress field along the interface can be decoupled into three individual modes: σ_{22} governed by K_I; σ_{12} governed by K_{II}; and σ_{23} governed by K_{III}.

However, such one-to-one relation does not exist for a bimaterial interfacial crack. As shown in Eq. 16, the oscillation index, ε, produces all the stress components along the interface for each mode governed by K_I, K_{II} or K_{III}. Therefore, the singular stress field cannot be decoupled into the three unique individual modes. Each of the singular stress fields along the interface is a function of the three stress intensity factors coupled by the oscillation index.

It is postulated that the fracture of an interfacial crack is determined by the singular stress field in the region near critical damage radii. The equivalent stress intensity factors $\hat{\mathbf{k}}_{r_o} \equiv \left\{\hat{K}_{II}, \hat{K}_I, \hat{K}_{III}\right\}^T$ at a characteristic radius r_o can be defined to characterize the singular stress field in the region near critical damage radii. [1]

$$\hat{\mathbf{k}}_{r_o} = \mathbf{Y}\left(r_o^{i\varepsilon}\right)\mathbf{k} \tag{17}$$

Then,

$$\boldsymbol{\tau}(x_1) = \frac{1}{\sqrt{2\pi x_1}} \frac{\mathbf{Y}\left(x_1^{i\varepsilon}\right)}{\mathbf{Y}\left(r_0^{i\varepsilon}\right)} \hat{\mathbf{k}} \approx \frac{1}{\sqrt{2\pi x_1}} \hat{\mathbf{k}} \tag{18}$$

It is seen from Eq. 18 that the equivalent stress intensity factor $\hat{\mathbf{k}}$ makes the coupling very weak near the characteristic radius r_o.

The damage radius for a mode I and mode II crack can be approximated with

$$\begin{aligned} r_I &= \frac{1}{2\pi}\left(\frac{K_{IC}}{\sigma_{22}^{ult}}\right)^2 \\ r_{II} &= \frac{1}{2\pi}\left(\frac{K_{IIC}}{\sigma_{12}^{ult}}\right)^2 \end{aligned} \tag{19}$$

Using the experimental data from Tab. 1, the damage radius of an interfacial crack in a T300-5208 graphite-epoxy laminate are $r_I = 0.05mm$ and $r_{II} = 0.24mm$. Since the magnitude of these two damage radius are close to the magnitude of the ply thickness ($t_{ply} = 0.127mm$), the ply thickness, t_{ply}, can be used as the characteristic length used in the defintion of the equivalent stress intensity factor, $\hat{\mathbf{k}}$.

With the ply thickness as the characteristic length, the coupling between (σ_{12} and $\hat{K}_I$) and (σ_{22} and $\hat{K}_{II}$) for the interface [0/90] are significantly reduced near the failure region. Along the

[1] It can be shown that the definition of $\hat{\mathbf{k}}_{r_o}$ is invariant of different measuring units [Rice (1988)].

Table 1: Experimental data for the critical energy release rate and their equivalent stress intensity factor of T300-5208

	G_{IC}	G_{IIC} (J/m2)	G_{IIIC}	K_{IC}	K_{IIC} (MPa $\sqrt{m}$)	K_{IIIC}	σ_{22}^{ult}	σ_{12}^{ult} (MPa)
Ref. 4	103	279-587	-	0.91	2.7-3.8	-	-	-
Ref. 5	88	154	-	0.84	2.0	-	-	-
Ref. 6*	-	-	1200	-	-	2.3	-	-
Ref. 22	-	-	-	-	-	-	50	75
Average	96	340	1200	0.88	2.9	2.3	50	75

* Experimental value for AS4/3501-6 graphite epoxy.

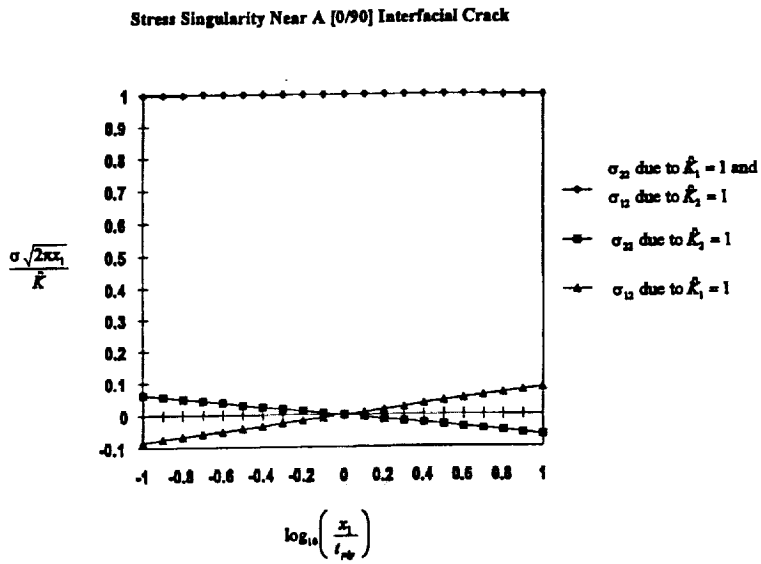

Figure 1: The decoupling of stress near the interfacial crack using ply thickness as the characteristic length for stress intensity factor definition

interface, $0.1t_{ply} < x_1 < 10t_{ply}$, the normalized coupling between the singular stress field and the stress intensity factor is less than 10% as shown in Fig. 1. As a result of this decoupling effect, the equivalent stress intensity factors of an interfacial crack has a similar physical interpretation with the stress intensity factor of a homogeneous crack near the damage region, in the sense that the strength of the singular stress field along the interface near the damage radius for mode I, mode II, and mode III are governed by $\hat{K}_I$, $\hat{K}_{II}$, and $\hat{K}_{III}$ respectively.

$$\begin{aligned} \sigma_{22}(x_1) &\approx \frac{\hat{K}_I}{\sqrt{2\pi x_1}}; \\ \sigma_{12}(x_1) &\approx \frac{\hat{K}_{II}}{\sqrt{2\pi x_1}}; \text{ for } |x_1 - t_{ply}| \leq \Omega; \Omega \to 0 \\ \sigma_{23}(x_1) &\approx \frac{\hat{K}_{III}}{\sqrt{2\pi x_1}} \end{aligned} \tag{20}$$

2.3 *A proposed stress intensity factor based fracture criterion*

Rice (1988) first suggested that the interface fracture toughness be defined by the total energy release rate and the phase angle of the stress intensity factor, $\psi = \tan^{-1}(K_{II}/K_I)$. Since then, many of the fracture toughness experiments for an interfacial crack are based on these two fracture parameters. Wang and Suo (1990) have used the Brazil nut specimen to obtain the interface toughness function for a Plexiglas/epoxy interface. Shanbhag et al. (1993) performed some fracture tests for perspex/epoxy, aluminum/epoxy and steel/epoxy interfaces using the compact tension specimen. Yuuki et al. (1994) have used the Brazil nut specimen to obtain the interface toughness function for an aluminum/epoxy interface. However, instead of using the energy release rate and the phase angle as the fracture criterion, Yuuki suggested a fracture criterion based on the quadratic mixture of the normalized stress intensity factor:

$$\left(\frac{\hat{K}_I}{K_{IC}}\right)^2 + \left(\frac{\hat{K}_{II}}{K_{IIC}}\right)^2 = const \tag{21}$$

where K_{IC} is the critical value for a pure $\hat{K}_I$ and $\hat{K}_{IIC}$ is the critical value for a pure $\hat{K}_{II}$. By normalizing the individual components of the stress intensity factors, the relative importance of each component is physically more intuitive. Unlike the fracture criterion based on the phase angle, this criterion can be easily extended to include the component $\hat{K}_{III}$ without the loss of the physical insight.

In the present work, the quadratic mixture of the stress intensity factor is modified to include the component $\hat{K}_{III}$. Furthermore, an additional factor of 0.85 for K_{IC} is added to reflect on the experimental observation [Yuuki et al. (1994)] that K_{IC} drops significantly when a small K_{II}/K_I exists as shown in Fig. 2. With this additional factor, the quadratic mixture theory would be valid for a wide range of K_{II}/K_I and this theory would deviate from the experimental results only when

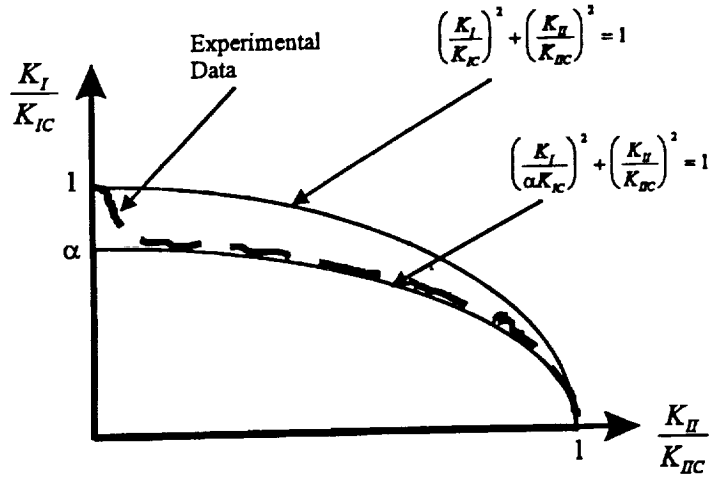

Figure 2: Fracture results for an interface crack

K_{II}/K_I is very small. The fracture criterion used to predict the onset of a delamination crack growth is as follows:

$$\hat{K}_0^2 = \left(\frac{\hat{K}_I}{0.85K_{IC}}\right)^2 + \left(\frac{\hat{K}_{II}}{K_{IIC}}\right)^2 + \left(\frac{\hat{K}_{III}}{K_{IIIC}}\right)^2 \tag{22}$$

$\hat{K}_0 \geq 1 \rightarrow$ interfacial crack failure

2.4 Interfacial fracture criterion for laminated composites

Consider an example of a delamination crack between the [0/90] laminate as shown in Fig. 3. The 0 lamina denotes that the fiber direction is along the out-of-plane direction, while the 90 lamina denotes that the fiber direction lies parallel to the crack. Since all of the experimental fracture data for the critical stress intensity factor, K_C, is based on a delamination crack in a unidirectional laminate, a question arises on whether the fracture data for [0/0] or [90/90] laminate could be used to predict the onset of delamination crack in the [0/90] laminate. Fig. 4a shows the stress distribution along the interface between the [0/90] laminate near the crack tip; and Fig. 4b shows the stress singularity near a crack in a homogeneous laminate ([0/0] or [90/90]) with the stress intensity factor of $\hat{K}_I/K_{IC} = 1$. These figures show that the stress distributions for both the cracks (bimaterial and homogeneous) are very similar except for a small region where there is considerable material nonlinearity and damage (defined as Zone 1 in the figures). Since the fracture of the delamination crack is assumed to be based on the stress concentration near the damage radius and the stress field near this damage radius for the interfacial crack is very similar to the homogeneous crack, the crit-

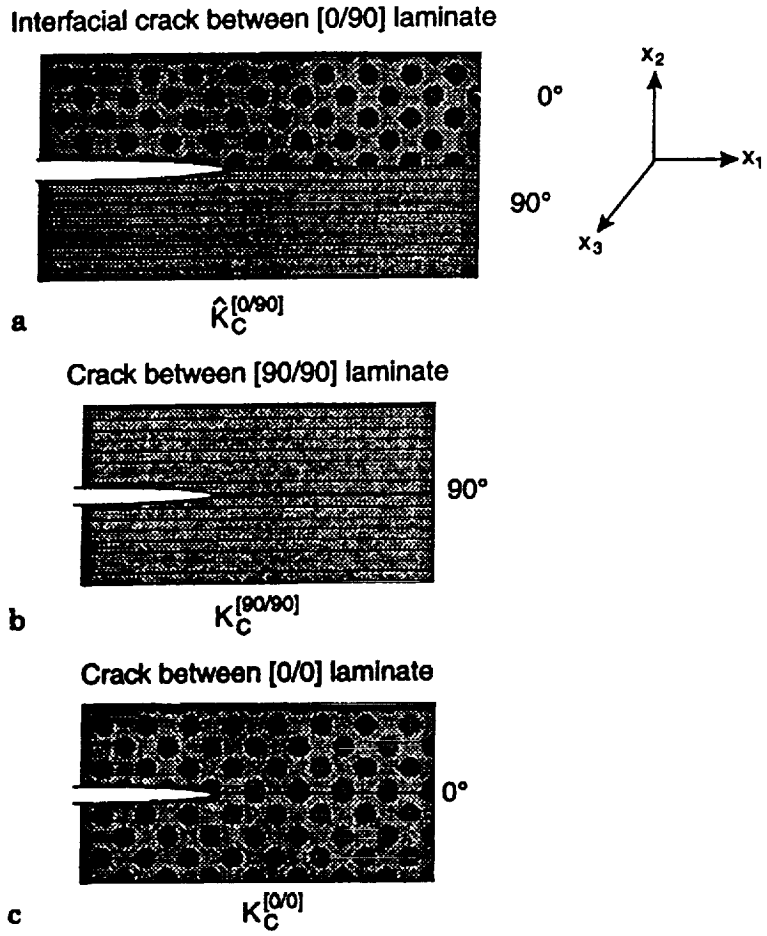

Figure 3: The critical stress intensity factor for an edge delamination crack between (**a**) [0/90] laminate, (**b**) [90/90] laminate, and (**c**) [0/0]laminate

ical stress intensity factor for [0/90] laminate, $\hat{K}_{[0/90]C}$, should be the related to the value of either $K_{[0/0]C}$ or $K_{[90/90]C}$. In addition, Lucas (1992) has performed some experiments on the fracture of a delamination crack in unidirectional laminates of different ply angle and found that the fracture toughness of a [90/90] laminate is less than a [0/0] laminate, $K_{[90/90]C} < K_{[0/0]C}$. Since a delamination crack between two dissimilar lamina can fracture at either the upper or lower lamina, it is reasonable to assume that the delamination crack would fracture at the material of lower fracture toughness. Hence, using this assumption, the critical stress intensity factor for [0/90] laminate, $\hat{K}_{[0/90]C}$, would be postulated as$K_{[90/90]C}$.

The nature of the stress field near a bimaterial interfacial crack is often defined by mixed-mode stress intensity factors. To deal with this, Chow and Atluri (1996) have suggested a mixed-mode fracture criterion based on the quadratic mixture of the mixed-mode stress intensity factors:

$$\left(\frac{\hat{K}_I}{0.85K_{IC}}\right)^2 + \left(\frac{\hat{K}_{II}}{K_{IIC}}\right)^2 + \left(\frac{\hat{K}_{III}}{K_{IIIC}}\right)^2 = \left(\theta_{fac}\hat{K}_0\right)^2 \qquad (23)$$
$$\hat{K}_0 \geq \hat{K}_C \rightarrow \text{interfacial crack failure}$$

where θ_{fac} is a non-dimensional constant dependent on the angle between the crack front and the fiber's direction. From the experiments performed by Lucas (1992), θ_{fac} for [90/90] laminate is 1.00, θ_{fac} for [45/45] is 1.15, and $\theta_{fac}$for [0/0] laminate is 1.61. This experimental result indicates that the [90/90] laminate has the lowest fracture toughness followed by the [45/45] laminate and then the [0/0] laminate. Using the assumptions discussed above, in which the bimaterial interfacial crack would fail at the material with a lower fracture toughness, the constant θ_{fac} for [45/90] and [45/0] would have the same values as [90/90] and [45/45] respectively. Therefore, θ_{fac} for [45/90] and [45/0] would have the values of 1.00 and 1.15 respectively. These two values would be used in the post-buckling analysis discussed in the next section. Since the normalized stress intensity factor, $\hat{K}_0$, is composed of mixed-mode stress intensity factors normalized with their respective critical stress intensity factors, $\hat{K}_0$ is a non-dimensional value. In the examples of composite laminates under uniaxial tension, Chow and Atluri (1996) have demonstrated that the critical stress intensity factor, $\hat{K}_C$, has the value of one when the delamination crack propagates in a 2-D fashion in which crack front remain straight. However, in the post-buckling failure of a stiffened laminated composite panel, the delamination crack propagates in an elliptical shape rather than in a 2-D fashion. As a result, the critical stress intensity factor, $\hat{K}_C$, to be used in the post-buckling analysis would have to be determined from the experimental data.

2.5 The effect of characteristic length

Chow and Atluri (1995) have studied the effect of characteristic length on the normalized stress intensity factor, $\hat{K}_0$. In the few examples they have considered, the value of $\hat{K}_0$ changes by only a few percent when the characteristic length changes by an order of magnitude. The relationship of mixed-mode stress intensity factors for different characteristic lengths is given by Qu and Bassani

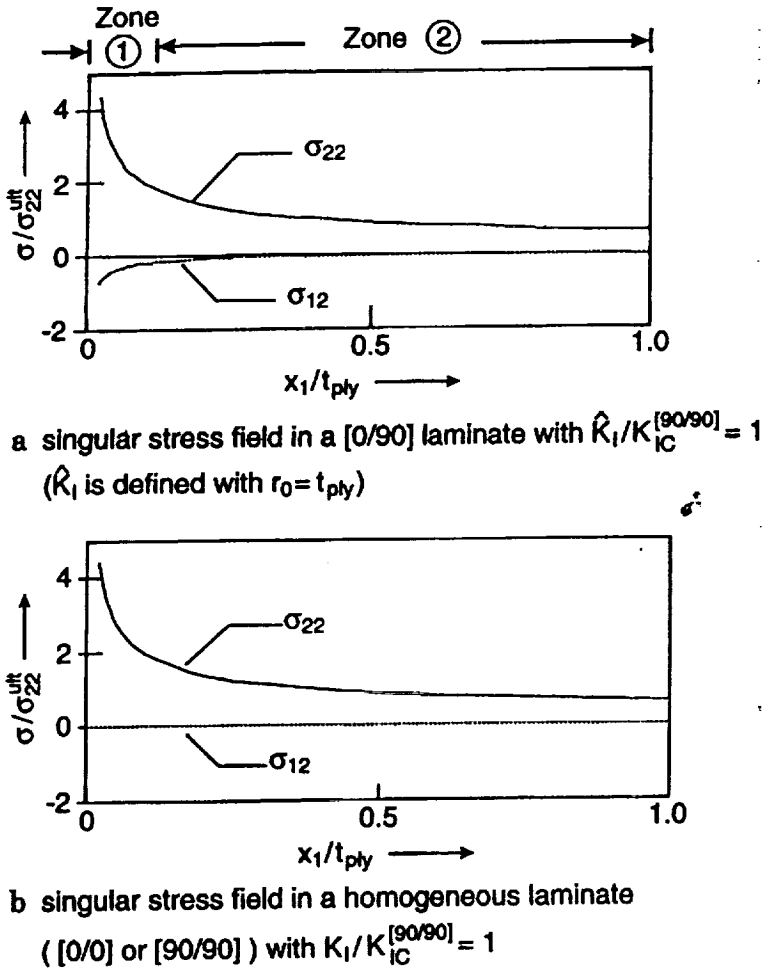

Figure 4: Stress distribution near the (a) interfacial and (b) homogeneous crack tip with Zone 1 being the damage zone (or nonlinear region) and Zone 2 being the region where the stress concentration influences the onset of crack propagation. Since the stress concentration at zone 2 are the same for both laminates, the fracture criterion for both laminates should be similar

(1993) as

$$\hat{\mathbf{k}}_{r_1} = \mathbf{Y}(r_1/r_0)\,\hat{\mathbf{k}}_{r_0} \tag{24}$$

where $\mathbf{Y}$ is a bimaterial matrix for the interfacial crack and $\hat{\mathbf{k}} = \left\{\hat{K}_{II}, \hat{K}_I, \hat{K}_{III}\right\}^T$

Consider a delamination crack between two angle-ply lamina, q and f, and the stress intensity factors, $\hat{k}_{r_0}$, are varied in a unit sphere:

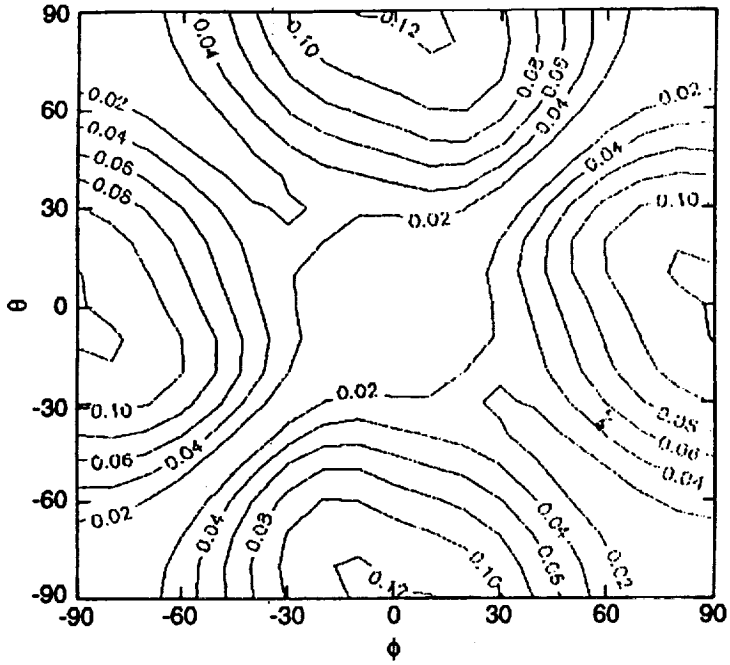

Figure 5: A contour plot of maximum change in the value of $\hat{K}_0$ for various ply lay-ups $[\theta, \phi]$, when the stress intensity factor, $\hat{K}_{r_0}$, are varied in the unit sphere with the characteristic length reduced by an order of a magnitude

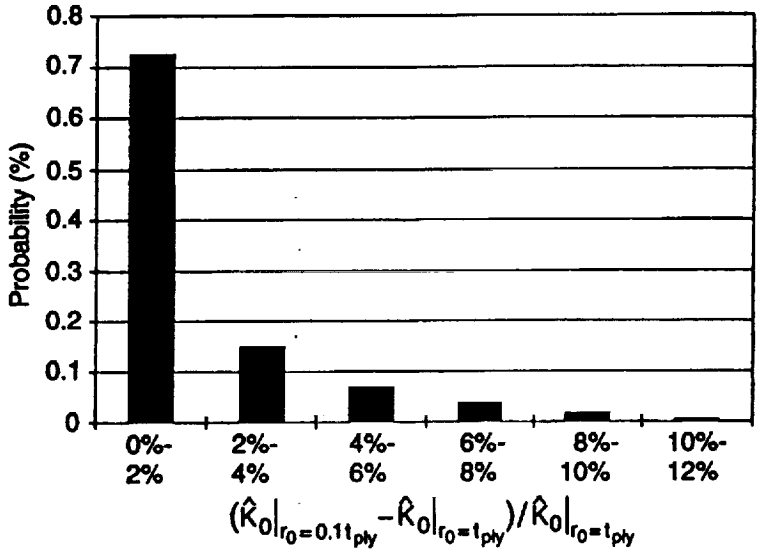

Figure 6: The probability of any combination sets of stress intensity factors, $\{\hat{K}_{II}, \hat{K}_I, \hat{K}_{III}\}^T$ of a delamination crack in any $[\theta/\phi]$ laminate which would result in the value of $\hat{K}_0$ to be changed by a certain factor when the definition of the characteristic length is reduced by an order of a magnitude

$$\begin{aligned} \hat{K}_I &= \sin(\alpha)\cos(\beta) \\ \hat{K}_{II} &= \sin(\alpha)\sin(\beta) \\ \hat{K}_{III} &= \cos(\alpha) \end{aligned} \tag{25}$$

where $-180° < \alpha, \beta < 180°$. By varying the stress intensity factors, $\hat{\mathbf{k}}_{r_0}$, in the unit sphere defined in Eq.25, a contour plot of the maximum change in the normalized stress intensity factor, $\hat{K}_0$, for various ply layups $-90° < \theta, \phi < 90°$, when the choice of characteristic length is reduced by an order of a magnitude is shown in Fig. 5. Except for the region near [0/90] interface, the effect of the characteristic length is quite small. Even for the [0/90] interface, the maximum change in $\hat{K}_0$ is less than 13%. To put things in perspective, a few percent change in $\hat{K}_0$ is really not very significant from an engineering point of view given the fact that most of the experimental data for delamination fracture would vary by 10%-20%. Moreover, the number of combinations of $\{\hat{K}_{II}, \hat{K}_I, \hat{K}_{III}\}^T$ and $[\theta/\phi]$ which gives significant change in the value of $\hat{K}_0$ is quite small; for 90% of the possible combinations of $\{\hat{K}_{II}, \hat{K}_I, \hat{K}_{III}\}^T$ and $[\theta/\phi]$, the value of $\hat{K}_0$ would change by no more 5% as shown in Fig. 6. Only 0.5% of the possible combinations would cause the value of $\hat{K}_0$ to differ by more than 10%.

2.6 Validation

The analysis presented in this section is based on the quasi-three-dimensional finite element method under generalized plane strain condition. This finite element analysis is based on eight-noded quadrilateral, isoparametric elements with 3 degrees of freedom per node. Standard quarter-point elements are used to model the interfacial crack tip. The numerical calculations performed in this section are for the T300-5208 graphite epoxy using the following elastic properties:

$E_L = 137GPa,\ E_T = E_Z = 10.8GPa,\ G_{ZT} = 3.36GPa,\ G_{ZL} = G_{TL} = 5.65GPa,\ \nu_{TZ} = 0.49,$
$\nu_{ZL} = \nu_{TL} = 0.238,\ t_{ply} = 0.127mm$

Here, L is the longitudinal direction, T is the transverse direction, and Z is the direction through the thickness. The experimental data for the critical energy release rate and the stress intensity factors of a mode I, II and III crack are listed in Tab. 1. These experimental results were obtained from double cantilever beam specimens with an initial crack front normal to the fibers' direction. In the present section, the critical stress intensity factors are based on the average of these experimental data. The fracture criterion used to predict the onset of delamination crack growth is based on the quadratic mixture of the normalized stress intensity factor defined in Eq. 22.

Mode I and II dominant crack

The stress intensity factor for a delamination crack in a laminate under tensile loading can be mode I and II dominant when the stacking sequence consists of 90^o plies being laid-up with plies of

Table 2: Laminates with mode I and II dominant delamination crack

Laminate	Crack between	$\frac{\varepsilon_{33}\hat{K}_I}{K_{IC}}$	$\frac{\varepsilon_{33}\hat{K}_{II}}{K_{IIC}}$	$\frac{\varepsilon_{33}\hat{K}_{III}}{K_{IIIC}}$	$\frac{\varepsilon_{33}^2 G_{total}}{G_{IC}}$
$[\pm 30/\pm 30/90/\overline{90}]_S$	$-30/90$	213	86	-11	5.8E4
$[\pm 45/0/90]_S$	$0/90$	146	29	-1.4	1.8E4
$[\pm 45_2/0_2/90_2]_S$	$0_2/90_2$	206	41	-2	3.5E4
$[\pm 45_3/0_3/90_3]_S$	$0_3/90_3$	253	50	-2.4	5.4E4
$[0/\pm 45/90]_S$	$-45/90$	80	65	-6.9	1.8E4

Laminate	Crack between	Predicted	Real	Error
Laminate	Crack between	Failure $\hat{\varepsilon}_{33}$	Failure ε_{33}	$\frac{\hat{\varepsilon}_{33}-\varepsilon_{33}}{\varepsilon_{33}}$
$[\pm 30/\pm 30/90/\overline{90}]_S$	$-30/90$ 0.0038	0.0035	8%	
$[\pm 45/0/90]_S$	$0/90$	0.0057	0.0056	3%
$[\pm 45_2/0_2/90_2]_S$	$0_2/90_2$	0.0041	0.0047	-12%
$[\pm 45_3/0_3/90_3]_S$	$0_3/90_3$	0.0033	0.0037	-10%
$[0/\pm 45/90]_S$	$-45/90$	0.0087	0.0080	3%

different angles. The mismatch of the lateral contraction due to the Poisson's effect between the 90^o plies and plies of different angles can sometimes be sufficient to cause the onset of delamination crack growth. Some of the examples for mode I and II dominant crack are listed in Tab. 2.

Tab. 3 lists the calculated stress intensity factor and energy release rate for two free-edge delamination cracks in a $[\pm 30/\pm 30/90/\overline{90}]_S$ laminate. The criterion based on the total energy release rate predicts that the crack would propagate along the second $[+30/-30]$ interface. However, the criterion based on stress intensity factor predicts the delamination crack would propagate along $[-30/90]$ interface which agrees with the experimental observation from O'Brien's research.

In Tab. 2, the criterion based on the total energy release rate predicts both $[0/\pm 45/90]_S$ and $[\pm 45/0/90]_S$ laminates would fail under the same tensile load since both laminates have a delamination crack of the same energy release rate. However, the criterion based on the stress intensity factor predicts the $[0/\pm 45/90]_S$ laminate would fail at a strain 50% greater than the $[\pm 45/0/90]_S$ laminate which agrees with the experimental results. Furthermore, Tab. 2 shows that the predicted failure strains, based on the stress intensity factors, of various laminates are within 12% from the experimental results [O'Brien (1982) and Sendeckyi et al. (1975)]. Hence, it validates the use of stress intensity factor as the fracture parameter to predict the onset of delamination growth.

Note that all the delamination cracks listed in Tab. 2 lie on top of a 90^o ply in which the normal of the crack front is in the fibers' direction. Moreover, the normal of the delamination crack front on the double cantilever beam specimen, in which the critical stress intensity factor is obtained, is also in the fibers' direction. Therefore, the critical stress intensity factor listed in Tab. 1 can

Table 3: Delamination cracks on a $[\pm 30/\pm 30/90/\overline{90}]_S$ laminate

Interface crack between	$\frac{\varepsilon_{33}K_I}{K_{IC}}$	$\frac{\varepsilon_{33}K_{II}}{K_{IIC}}$	$\frac{\varepsilon_{33}K_{III}}{K_{IIIC}}$	$\hat{K}_0$	$\frac{\varepsilon_{33}^2 G_{total}}{G_{IC}}$
second $+30/-30$	143	55	108	207	7.0E4
$-30/90$	213	86	-11	265	5.8E4

be directly used in the examples listed in Tab. 2. However, the critical stress intensity factors do change if the normal of the crack front deviates from the fibers' direction. The experiment by Lucas (1992) has shown that as the angle between the normal of the crack front and the fibers' direction increased, the critical stress intensity factor would increase as well. Hence, some adjustment on the fracture criterion would be required when the interfacial crack does not lie either on top or bottom of a 90^o ply.

Mode III dominant crack

When a laminate of $\pm\theta$ layers, where θ is between 0^o and 90^o, is under tensile loading, the coupling between the normal strain, ε_{33}, and the transverse shear stress, σ_{23}, are directly opposite for $+\theta$ and $-\theta$ layers. As a result, the stress intensity factor of a delamination crack between $\pm\theta$ layers is often mode III dominant when the laminate is under tensile loading. In this study, the fiber orientations of 10^o, 30^o, and 45^o are considered. The stacking sequence of the laminate is either $[(\pm\theta)_2]_S$ (alternating) or $[\theta_2/-\theta_2]_S$ (clustered).

Tab. 4 lists the calculated stress intensity factors and the comparisons between the predicted failure strain and the experimental results by Herakovich (1982). There are several explanations that can be given for the considerable disparity between these results. For $[(\pm 10)_2]_S$ and $[(\pm 30)_2]_S$ laminate, Herakovich observed no delamination propagation when these laminates failed. In fact, using the Tsai-Hill failure theory, we can see that these laminates failed because the stresses on each lamina exceeded the ultimate stress. The reasons for the prediction errors for other laminates can be attributed to the wrong assumption used in describing the crack front. Observations from the experiments for these stacking sequences show that the delamination propagates in a triangular shape rather than in a straight crack front shown in Fig. 8. Hence, to fully model the delamination growth for these laminates, a full three-dimensional model must be used instead. Furthermore, material nonlinearity must also be taken into account in analyzing the failure of $\pm 45^o$ laminate.

Table 4: Laminates with mode III dominant delamination crack

Laminate	Interface crack between	$\frac{\varepsilon_{33}\hat{K}_I}{K_{IC}}$	$\frac{\varepsilon_{33}\hat{K}_{II}}{K_{IIC}}$	$\frac{\varepsilon_{33}\hat{K}_{III}}{K_{IIIC}}$	$\frac{\varepsilon_{33}^2 G_{total}}{G_{IC}}$
$[(\pm 10)_2]_S$	second $+10/-10$	-2.6	2.2	100	3.9E4
$[(\pm 30)_2]_S$	second $+30/-30$	11	12	87	2.3E4
$[(\pm 45)_2]_S$	second $+45/-45$	6.9	8	31	3.8E4
$[\pm(10_2)]_S$	$+10_2/-10_2$	-8	0.4	173	1.2E4
$[\pm(30_2)]_S$	$+30_2/-30_2$	-7.5	0.0	160	7.3E4
$[\pm(45_2)]_S$	$+45_2/-45_2$	-2.6	0.0	61	1.3E4

Laminate	Interface crack between	Predicted Failure $\hat{\varepsilon}_{33}$	Real Failure ε_{33}	Error $\frac{\hat{\varepsilon}_{33}-\varepsilon_{33}}{\varepsilon_{33}}$
$[(\pm 10)_2]_S$	second $+10/-10$	0.0100	0.0070	43%
$[(\pm 30)_2]_S$	second $+30/-30$	0.0113	0.0117	-3%
$[(\pm 45)_2]_S$	second $+45/-45$	0.0301	0.0158	90%
$[\pm(10_2)]_S$	$+10_2/-10_2$	0.0058	0.0049	18%
$[\pm(30_2)]_S$	$+30_2/-30_2$	0.0063	0.0067	-7%
$[\pm(45_2)]_S$	$+45_2/-45_2$	0.0163	0.0097	68%

3 A Virtual Crack Closure Integral Method for the Evaluation of Mixed-mode SIF for Interfacial Cracks

This section documents the development of a virtual crack closure integral method for the evaluation of mixed-mode stress intensity factors for an interfacial crack between two dissimilar isotropic and anisotropic mediums. The mixed-modes stress intensity factors can be related to a set of energy release rates by the use of a coupled mixed-mode energy release rate. Therefore, the stress intensity factors can be easily solved for once the mixed-mode energy release rates are evaluated from a finite element solution.

The modified crack closure integral method has become a useful technique in calculating the fracture parameters of a crack lying in a homogeneous isotropic domain. This method is attractive for many researchers and engineers because of its simplicity and effectiveness in calculating the individual components of the mixed-mode stress intensity factors and the energy release rates. The Irwin's virtual crack closure method was first applied by Rybicki and Kanninen (1977) with 4-noded isoparametric finite elements to compute the mixed-mode energy release rates of a crack lying in a homogeneous isotropic domain. To improve on the accuracy of the computed fracture parameters, Raju (1987) has further extended this method for higher order and singular finite elements.

To calculate the stress intensity factors for an interfacial crack in an isotropic bimaterial con-

tinuum, Lin and Mar (1976) have developed the hybrid stress element method, and Kathiresan and Atluri (1978) have developed the hybrid displacement element method. Using the mutual integral, M, Cho et al. (1994) have calculated the stress intensity factors for an interfacial crack between t-wo dissimilar isotropic media from the stress results of an ordinary finite element analysis (without the need to develop a hybrid element). Chow et al. (1995) have further extended both the hybrid stress element method and the mutual integral method to compute the stress intensity factors for an interfacial crack between dissimilar anisotropic media. However, these methods required the knowledge of the asymptotic stress and displacement field around the interfacial crack tip. Since the asymptotic stress and displacement field involve complex numbers, the calculation of the stress intensity factors using these methods require a considerable programming effort.

The computation of the stress intensity factors for an interfacial crack can be significantly simplified, using the virtual crack closure integral approach. The stress intensity factors for an interfacial crack can be computed from the crack opening displacements and the nodal forces at and ahead of the crack tip. The simple formula to calculate the stress intensity factors for an interfacial crack are given in three separate categories: an isotropic bimaterial continuum, an orthotropic bimaterial continuum, and an anisotropic bimaterial continuum.

3.1 Virtual crack closure integral method

The work required to extend a crack by an infinitesimal distance Δ is equal to the work required to close the crack to its original length [Irwin (1958)]. Thus, the energy release rate for mode I and mode II deformations can be expressed as

$$G_I = \frac{1}{2\Delta}\int_0^{\Delta} \sigma_{22}(r)\,\delta_2(\Delta - r)\,dr \tag{26}$$

$$G_{II} = \frac{1}{2\Delta}\int_0^{\Delta} \sigma_{12}(r)\,\delta_1(\Delta - r)\,dr$$

where σ is the stress distribution ahead of the crack tip, and δ is the crack opening displacement behind the crack tip. Here, the crack-axis is along the x_1 axis and normal to the x_2 axis as indicated in Fig. 7.

The procedure to obtain these energy release rates from finite element solutions were given by Rybicki and Kanninen (1977) and Raju (1987). For quarter-point singular elements (shown in Fig. 7), the energy release rate for mode I can be obtained from the nodal forces and displacements near the crack tip (along the crack-axis) with the virtual crack closure technique as

$$\begin{aligned} G_I = -\tfrac{1}{2\Delta}\Big[& F^{(1)}_{2\,[i]}\left\{ t_{11}\left(u^{(1)}_{2\,[m]} - u^{(2)}_{2\,[m]}\right) + t_{12}\left(u^{(1)}_{2\,[l]} - u^{(2)}_{2\,[l]}\right)\right\} \\ & + F^{(1)}_{2\,[j]}\left\{ t_{21}\left(u^{(1)}_{2\,[m]} - u^{(2)}_{2\,[m]}\right) + t_{22}\left(u^{(1)}_{2\,[l]} - u^{(2)}_{2\,[l]}\right)\right\}\Big] \end{aligned} \tag{27}$$

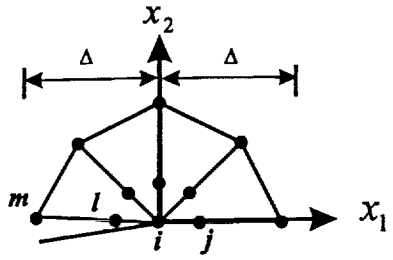

Figure 7: Quarter-point singular elements surrounding the crack tip

$$G_{II} = -\frac{1}{2\Delta}\left[F^{(1)}_{1\,[i]}\left\{t_{11}\left(u^{(1)}_{1\,[m]} - u^{(2)}_{1\,[m]}\right) + t_{12}\left(u^{(1)}_{1\,[l]} - u^{(2)}_{1\,[l]}\right)\right\}\right.$$
$$\left. + F^{(1)}_{1\,[j]}\left\{t_{21}\left(u^{(1)}_{1\,[m]} - u^{(2)}_{1\,[m]}\right) + t_{22}\left(u^{(1)}_{1\,[l]} - u^{(2)}_{1\,[l]}\right)\right\}\right] \tag{28}$$

where

$$\begin{aligned} t_{11} &= 6 - \frac{3\pi}{2};\ t_{12} = 6\pi - 20; \\ t_{21} &= \frac{1}{2};\quad t_{22} = 1. \end{aligned} \tag{29}$$

The symbol $F^{(1)}_{2\,[i]}$ represents the nodal force computed from the singular elements in material 1 in the direction parallel to x_2 axis at node $[i]$ as shown in Fig. 7.

For a crack in a homogeneous domain, there exists no coupling between $\{\sigma_{22}(r)$ and $\delta_1(\Delta - r)\}$ and between $\{\sigma_{12}(r)$ and $\delta_2(\Delta - r)\}$. However, these couplings do exist for an interfacial crack between two dissimilar media. Because of such couplings, the calculated energy release rates G_I and G_{II} are dependent upon the value of the distance Δ. As a result, Raju et al. (1988) as well as Sun and Jih (1987) have found that the calculated energy release rates using the virtual crack closure integral method are dependent upon the mesh refinement of the crack tip elements surrounding an interfacial crack. To resolve this problem, Chow and Atluri (1995) has introduced a coupled energy release rate G_{I-II} to simplify the relationships between the stress intensity factors and the mixed-mode energy release rates (obtained through virtual crack integral method). The coupled energy release rate G_{I-II} is defined as:

$$G_{I-II} = \frac{1}{2\Delta}\int_0^{\Delta}\left[\sigma_{12}(r)\,\delta_2(\Delta - r) + \sigma_{22}(r)\,\delta_1(\Delta - r)\right]dr \tag{30}$$

G_{I-II} can be evealuted for the nodal forces and displacments at the nodes of the quater-point singular elements at the crack tip.

$$
\begin{aligned}
G_{I-II} = -\tfrac{1}{2\Delta}\Big[& F_{1\,[i]}^{(1)}\left\{t_{11}\left(u_{2\,[m]}^{(1)} - u_{2\,[m]}^{(2)}\right) + t_{12}\left(u_{2\,[l]}^{(1)} - u_{2\,[l]}^{(2)}\right)\right\} \\
& + F_{1\,[j]}^{(1)}\left\{t_{21}\left(u_{2\,[m]}^{(1)} - u_{2\,[m]}^{(2)}\right) + t_{22}\left(u_{2\,[l]}^{(1)} - u_{2\,[l]}^{(2)}\right)\right\} \\
& + F_{2\,[i]}^{(1)}\left\{t_{11}\left(u_{1\,[m]}^{(1)} - u_{1\,[m]}^{(2)}\right) + t_{12}\left(u_{1\,[l]}^{(1)} - u_{1\,[l]}^{(2)}\right)\right\} \\
& + F_{2\,[j]}^{(1)}\left\{t_{21}\left(u_{1\,[m]}^{(1)} - u_{1\,[m]}^{(2)}\right) + t_{22}\left(u_{1\,[l]}^{(1)} - u_{1\,[l]}^{(2)}\right)\right\}\Big]
\end{aligned}
\tag{31}
$$

Once these energy release rates are calculated, the stress intensity factors for an interfacial crack can be easily computed from a linear equation. The detailed relations for between stress intensity factors and energy release rates for (i) an isotropic bimaterial continuum, (ii) an orthotropic bimaterial continuum, and (iii) an anisotropic bimaterial continuum, are discussed in the remaining part of this section.

3.2 Interfacial crack in an isotropic bimaterial continuum

For an interfacial crack between dissimilar isotropic media, there exists an oscillation index which causes the oscillation of stress and displacement near the crack tip. This oscillation index is defined as

$$
\varepsilon = \frac{1}{2\pi}\ln\left[\frac{\mu^{(1)} + \mu^{(2)}\kappa^{(1)}}{\mu^{(2)} + \mu^{(1)}\kappa^{(2)}}\right] \tag{32}
$$

where μ is shear modulus and $\kappa = 3 - 4\nu$ for plane strain and $\kappa = (3-\nu)/(1+\nu)$ for plane stress. The stress field along the interface at a distance r ahead of a crack tip is given by

$$
\sigma_{22} + i\sigma_{12} = \frac{K}{\sqrt{2\pi r}} r^{i\varepsilon} \tag{33}
$$

where $K = K_I + iK_{II}$ is the complex stress intensity factor. The crack opening displacements at a distance r behind the crack tip are given by:

$$
\delta_2 + i\delta_1 = \frac{c^{(1)} + c^{(2)}}{2\sqrt{2\pi}\,(1+2i\varepsilon)\,cosh\,(\pi\varepsilon)} K\sqrt{r}\, r^{i\varepsilon} \tag{34}
$$

where the compliance parameters, c, are

$$
c^{(1)} = \frac{\kappa^{(1)} + 1}{\mu^{(1)}},\quad c^{(2)} = \frac{\kappa^{(2)} + 1}{\mu^{(2)}} \tag{35}
$$

Substituting Eq.33 and Eq.34 into Eq. 26-30, the energy release rates can be defined as functions of the complex stress intensity factor, K.

$$G_I = \frac{c^{(1)} + c^{(2)}}{8\pi \cosh(\pi\varepsilon)} \lim Re \left[\frac{\Delta^{2i\varepsilon} K^2}{1+2i\varepsilon} I_1 + \frac{|K|^2}{1+2i\varepsilon} I_2 \right] \tag{36}$$

$$G_{II} = \frac{c^{(1)} + c^{(2)}}{8\pi \cosh(\pi\varepsilon)} \lim Re \left[-\frac{\Delta^{2i\varepsilon} K^2}{1+2i\varepsilon} I_1 + \frac{|K|^2}{1+2i\varepsilon} I_2 \right] \tag{37}$$

$$G_{I-II} = \frac{c^{(1)} + c^{(2)}}{4\pi \cosh(\pi\varepsilon)} \lim Im \left[\frac{\Delta^{2i\varepsilon} K^2}{1+2i\varepsilon} I_1 \right] \tag{38}$$

where

$$I_1 = \int_0^{\pi/2} \cos^2\omega (\sin\omega \cos\omega)^{2i\varepsilon} d\omega \tag{39}$$

$$I_2 = \int_0^{\pi/2} \cos^2\omega (\cos\omega / \sin\omega)^{2i\varepsilon} d\omega = \frac{\pi(1+2i\varepsilon)}{4\cosh(\pi\varepsilon)} \tag{40}$$

The integral I_1 in Eq.39 is a Beta function and can be evaluated numerically using numerical integration scheme. To simplify the relations between the stress intensity factors and the energy release rates, the integral I_1 is approximated with

$$I_1 \approx \frac{\pi}{\cosh(\pi\varepsilon)} \left(\frac{1}{4} - \frac{1}{6}\varepsilon^2 - i\frac{5}{7}\varepsilon \right) \tag{41}$$

This approximation is valid for the realistic range of e. Dundurs (1969) has shown that for an interfacial crack in isotropic bimaterial continuum, the absolute value for the oscillation index, ε, has to less than or equal to $(1/2\pi)\ln 3$. The error of the approximation in Eq. 41 for this range normalized with $\int_0^{\pi/2} \cos^2\omega d\omega$ is less than 0.5%.

Substituting Eq. 39-41 into Eq. 36-38 and rearranging the equations, the simple relationship between the stress intensity factors and the energy release rates are obtained:

$$\begin{bmatrix} a_{11}a_{21} + a_{12}^2 & a_{22}a_{21} - a_{12}^2 \\ a_{22}a_{21} - a_{12}^2 & a_{11}a_{21} + a_{12}^2 \end{bmatrix} \begin{Bmatrix} K_I^2 \\ K_{II}^2 \end{Bmatrix} = \lambda \begin{Bmatrix} a_{21}G_I - a_{12}G_{I-II} \\ a_{21}G_{II} + a_{12}G_{I-II} \end{Bmatrix} \tag{42}$$

where

$$\lambda = \frac{32\cosh^2(\pi\varepsilon)\left(1+4\varepsilon^2\right)}{c^{(1)} + c^{(2)}} \tag{43}$$

$$a_{11} = \left(1+4\varepsilon^2\right) + \left(1-\frac{134}{21}\varepsilon^2\right)\cos\left[2\varepsilon\ln\left(\Delta\right)\right] + \left(\frac{34}{7}\varepsilon - \frac{4}{3}\varepsilon^3\right)\sin\left[2\varepsilon\ln\left(\Delta\right)\right] \tag{44}$$

$$a_{12} = 2\left\{\left(\frac{34}{7}\varepsilon - \frac{4}{3}\varepsilon^3\right)\cos\left[2\varepsilon\ln\left(\Delta\right)\right] - \left(1-\frac{134}{21}\varepsilon^2\right)\sin\left[2\varepsilon\ln\left(\Delta\right)\right]\right\} \tag{45}$$

$$a_{22} = \left(1+4\varepsilon^2\right) - \left(1-\frac{134}{21}\varepsilon^2\right)\cos\left[2\varepsilon\ln\left(\Delta\right)\right] - \left(\frac{34}{7}\varepsilon - \frac{4}{3}\varepsilon^3\right)\sin\left[2\varepsilon\ln\left(\Delta\right)\right] \tag{46}$$

$$a_{21} = 4\left\{\left(1-\frac{134}{21}\varepsilon^2\right)\cos\left[2\varepsilon\ln\left(\Delta\right)\right] + \left(\frac{34}{7}\varepsilon - \frac{4}{3}\varepsilon^3\right)\sin\left[2\varepsilon\ln\left(\Delta\right)\right]\right\} \tag{47}$$

Hence, the square of the stress intensity factors, K_I^2 and K_{II}^2, can be easily solved from the linear equation in Eq.42. The signs for the stress intensity factors, K_I and K_{II}, can be ascertained from the crack opening displacements. For a crack in a homogeneous isotropic continuum, $\varepsilon = 0$, resulting in a considerable simplification of Eqs. 43-47, i.e.:

$$K_I^2 = \frac{2}{c}G_I,\ K_{II}^2 = \frac{2}{c}G_{II} \tag{48}$$

3.3 Interfacial crack in an orthotropic bimaterial continuum

For an orthotropic bimaterial aligned with the interface crack coordinate system (e.g., a 0/90 degree laminate where the fibers are parallel to the crack front in one material and perpendicular in the other), the stress field along the interface at a distance r ahead of a crack tip is given by Qu and Bassani (1993) as:

$$\beta_2^{1/2}\sigma_{22} + i\beta_1^{1/2}\sigma_{12} = \frac{\beta_2^{1/2}K_I + i\beta_1^{1/2}K_{II}}{\sqrt{2\pi r}}r^{i\varepsilon} \tag{49}$$

and the crack opening displacements at a distance r behind the crack tip are

$$\beta_1^{1/2}\delta_2 + i\beta_2^{1/2}\delta_1 = \frac{\left(s^{(1)} - s^{(2)}\right)\sqrt{2\pi r}r^{i\varepsilon}}{\pi\beta\left(1+2i\varepsilon\right)\cosh\left(\pi\varepsilon\right)}\left(\beta_2^{1/2}K_I + i\beta_1^{1/2}K_{II}\right) \tag{50}$$

The bimaterial constants

$$\varepsilon = \frac{1}{2\pi}\ln\left(\frac{1+\beta}{1-\beta}\right) \tag{51}$$

$$\beta = \sqrt{\beta_1\beta_2} \tag{52}$$

$$\beta_1 = \frac{s^{(1)} - s^{(2)}}{s^{(1)}\rho^{(1)}/\eta^{(1)} + s^{(2)}\rho^{(2)}/\eta^{(2)}} \tag{53}$$

$$\beta_2 = \frac{s^{(1)} - s^{(2)}}{s^{(1)}/\eta^{(1)} + s^{(2)}/\eta^{(2)}} \tag{54}$$

are obtained from the orthotropic material constants

$$s = \left[C_{1122} + \sqrt{C_{1111}C_{2222}}\right]^{-1} \tag{55}$$

$$\eta = \left[\frac{C_{1212}\left(\sqrt{C_{1111}C_{2222}} - C_{1122}\right)}{C_{2222}\left(2C_{1212} + C_{1122} + \sqrt{C_{1111}C_{2222}}\right)}\right]^{1/2} \tag{56}$$

$$\rho = \sqrt{\frac{C_{1111}}{C_{2222}}} \tag{57}$$

where C_{ijkl} is the stiffness matrix that relates the stresses, σ_{ij}, to strains, ε_{kl}

$$\sigma_{ij} = \sum_{k=1}^{3}\sum_{l=1}^{2} C_{ijkl}\varepsilon_{kl} \tag{58}$$

By substituting Eq.49-50 into Eq.26-30, the simple relationship between the stress intensity factors and the energy release rates are obtained:

$$\begin{bmatrix} a_{11}a_{21} + a_{12}^2 & a_{22}a_{21} - a_{12}^2 \\ a_{22}a_{21} - a_{12}^2 & a_{11}a_{21} + a_{12}^2 \end{bmatrix} \begin{Bmatrix} \beta_2 K_I^2 \\ \beta_1 K_{II}^2 \end{Bmatrix} = \begin{Bmatrix} a_{21}\lambda_1 G_I - a_{12}\lambda_2 G_{I-II} \\ a_{21}\lambda_1 G_{II} + a_{12}\lambda_2 G_{I-II} \end{Bmatrix} \tag{59}$$

where

$$\lambda_1 = \frac{8\cosh^2(\pi\varepsilon)\left(1 + 4\varepsilon^2\right)\beta^2}{s^{(1)} - s^{(2)}} \tag{60}$$

$$\lambda_2 = \frac{16\cosh^2(\pi\varepsilon)\left(1 + 4\varepsilon^2\right)\beta^3}{\left(s^{(1)} - s^{(2)}\right)\left(\beta_1 + \beta_2\right)} \tag{61}$$

The square of the stress intensity factors, K_I^2 and K_{II}^2, can be easily solved from the linear equation in Eq.59. The signs for the stress intensity factors, K_I and K_{II}, can be ascertained from the crack opening displacements. Once again, for a homogeneous orthotropic continuum, the relationship between the stress intensity factors and energy release rates are reduced to

$$K_I^2 = \frac{2\eta}{s\rho} G_I,\ K_{II}^2 = 2\eta G_{II} \tag{62}$$

3.4 Interfacial crack in an anisotropic bimaterial continuum

For a general anisotropic bimaterial continuum, the asymptotic stress field along the interface at a distance r ahead of a crack tip is given by

$$\tau(r) = \frac{1}{\sqrt{2\pi r}} \boldsymbol{Y}\left(r^{i\varepsilon}\right)\ \boldsymbol{k} \tag{63}$$

and the crack opening displacements at a distance r behind the crack tip are

$$\delta(r) = \sqrt{2r/\pi}\, \boldsymbol{DY}\left[\frac{r^{i\varepsilon}}{(1+2i\varepsilon)\cosh(\pi\varepsilon)}\right] \boldsymbol{k} \tag{64}$$

where $\tau = \{\sigma_{21}, \sigma_{22}, \sigma_{23}\}^T$, $\delta = \{\delta_1, \delta_2, \delta_3\}^T$ and $\boldsymbol{k} = \{K_{II}, K_I, K_{III}\}^T$. The bimaterial matrices $\boldsymbol{D}$ and $\boldsymbol{W}$ can be written in terms of the anisotropic matrices $\boldsymbol{L}$ and $\boldsymbol{S}$ (Eqs. 5 and 5)

$$\boldsymbol{D} = \boldsymbol{L}^{(1)-1} + \boldsymbol{L}^{(2)-1} \tag{65}$$

$$\boldsymbol{W} = \boldsymbol{S}^{(1)}\boldsymbol{L}^{(1)-1} - \boldsymbol{S}^{(2)}\boldsymbol{L}^{(2)-1} \tag{66}$$

and the bimaterial function $\boldsymbol{Y}$ defined 6 in can be rewritten as

$$\boldsymbol{Y}\left(r^{i\varepsilon}\right) = \boldsymbol{V}^{(1)} + \sin(\varepsilon \ln r)\boldsymbol{V}^{(2)} + \cos(\varepsilon \ln r)\boldsymbol{V}^{(3)} \tag{67}$$

$$\boldsymbol{DY}\left[\frac{r^{i\varepsilon}}{(1+2i\varepsilon)\cosh(\pi\varepsilon)}\right] = \boldsymbol{U}^{(1)} + \sin(\varepsilon \ln r)\,\boldsymbol{U}^{(2)} + \cos(\varepsilon \ln r)\,\boldsymbol{U}^{(3)} \tag{68}$$

$$\beta = \left\{-\frac{1}{2} tr\left(\left[\boldsymbol{D}^{-1}\boldsymbol{W}\right]^2\right)\right\}^{\frac{1}{2}} \tag{69}$$

in which the matrices

$$\begin{aligned}
&\boldsymbol{V}^{(1)} = \boldsymbol{I} + \tfrac{1}{\beta^2}\left(\boldsymbol{D}^{-1}\boldsymbol{W}\right)^2,\quad \boldsymbol{V}^{(2)} = -\tfrac{1}{\beta}\boldsymbol{D}^{-1}\boldsymbol{W},\quad \boldsymbol{V}^{(3)} = -\tfrac{1}{\beta^2}\left(\boldsymbol{D}^{-1}\boldsymbol{W}\right)^2 \\
&\boldsymbol{U}^{(1)} = \boldsymbol{D} + \tfrac{1}{\beta^2}\boldsymbol{W}\boldsymbol{D}^{-1}\boldsymbol{W},\quad \boldsymbol{U}^{(2)} = -\frac{1}{\left(1+4\varepsilon^2\right)\cosh(\pi\varepsilon)\beta}\left[\boldsymbol{W} + \tfrac{2\varepsilon}{\beta}\boldsymbol{W}\boldsymbol{D}^{-1}\boldsymbol{W}\right], \\
&\boldsymbol{U}^{(3)} = \frac{1}{\left(1+4\varepsilon^2\right)\cosh(\pi\varepsilon)\beta}\left[2\varepsilon\boldsymbol{W} - \tfrac{1}{\beta}\boldsymbol{W}\boldsymbol{D}^{-1}\boldsymbol{W}\right]
\end{aligned} \tag{70}$$

A procedure similar in the case of an isotropic bimaterial continuum can also be applied in the case of an anisotropic bimaterial continuum. For a general anisotropic bimaterial continuum, three additional energy release rates are required,

$$\begin{aligned} G_{III} &= \tfrac{1}{2\Delta}\int_0^{\Delta}\sigma_{23}(r)\,\delta_3(\Delta-r)\,dr \\ &= -\tfrac{1}{2\Delta}\left[F_{3\,[i]}^{(1)}\left\{t_{11}\left(u_{3\,[m]}^{(1)}-u_{3\,[m]}^{(2)}\right)+t_{12}\left(u_{3\,[l]}^{(1)}-u_{3\,[l]}^{(2)}\right)\right\}\right. \\ &\left.+F_{3\,[j]}^{(1)}\left\{t_{21}\left(u_{3\,[m]}^{(1)}-u_{3\,[m]}^{(2)}\right)+t_{22}\left(u_{3\,[l]}^{(1)}-u_{3\,[l]}^{(2)}\right)\right\}\right] \end{aligned} \tag{71}$$

$$\begin{aligned} G_{II-III} &= \frac{1}{2\Delta}\int_0^{\Delta}\left[\sigma_{12}(r)\,\delta_3(\Delta-r)+\sigma_{23}(r)\,\delta_1(\Delta-r)\right]dr \\ &= -\frac{1}{2\Delta}\left[F_{1\,[i]}^{(1)}\left\{t_{11}\left(u_{3\,[m]}^{(1)}-u_{3\,[m]}^{(2)}\right)+t_{12}\left(u_{3\,[l]}^{(1)}-u_{3\,[l]}^{(2)}\right)\right\}\right. \\ &\quad+F_{1\,[j]}^{(1)}\left\{t_{21}\left(u_{3\,[m]}^{(1)}-u_{3\,[m]}^{(2)}\right)+t_{22}\left(u_{3\,[l]}^{(1)}-u_{3\,[l]}^{(2)}\right)\right\} \\ &\quad+F_{3\,[i]}^{(1)}\left\{t_{11}\left(u_{1\,[m]}^{(1)}-u_{3\,[m]}^{(2)}\right)+t_{12}\left(u_{1\,[l]}^{(1)}-u_{3\,[l]}^{(2)}\right)\right\} \\ &\left.\quad+F_{3\,[j]}^{(1)}\left\{t_{21}\left(u_{1\,[m]}^{(1)}-u_{1\,[m]}^{(2)}\right)+t_{22}\left(u_{1\,[l]}^{(1)}-u_{1\,[l]}^{(2)}\right)\right\}\right] \end{aligned} \tag{72}$$

$$\begin{aligned} G_{I-III} &= \frac{1}{2\Delta}\int_0^{\Delta}\left[\sigma_{22}(r)\,\delta_3(\Delta-r)+\sigma_{23}(r)\,\delta_2(\Delta-r)\right]dr \\ &= -\frac{1}{2\Delta}\left[F_{2\,[i]}^{(1)}\left\{t_{11}\left(u_{3\,[m]}^{(1)}-u_{3\,[m]}^{(2)}\right)+t_{12}\left(u_{3\,[l]}^{(1)}-u_{3\,[l]}^{(2)}\right)\right\}\right. \\ &\quad+F_{2\,[j]}^{(1)}\left\{t_{21}\left(u_{3\,[m]}^{(1)}-u_{3\,[m]}^{(2)}\right)+t_{22}\left(u_{3\,[l]}^{(1)}-u_{3\,[l]}^{(2)}\right)\right\} \\ &\quad+F_{3\,[i]}^{(1)}\left\{t_{11}\left(u_{2\,[m]}^{(1)}-u_{2\,[m]}^{(2)}\right)+t_{12}\left(u_{2\,[l]}^{(1)}-u_{2\,[l]}^{(2)}\right)\right\} \\ &\left.\quad+F_{3\,[j]}^{(1)}\left\{t_{21}\left(u_{2\,[m]}^{(1)}-u_{2\,[m]}^{(2)}\right)+t_{22}\left(u_{2\,[l]}^{(1)}-u_{2\,[l]}^{(2)}\right)\right\}\right] \end{aligned} \tag{73}$$

$$\tag{74}$$

Two additional integrals are introduced,

$$I_3=\int_0^{\pi/2}\cos^2\theta\,(\cos\theta)^{2i\varepsilon}\,d\theta\approx\frac{\pi}{4}-\frac{17}{100}\varepsilon^2-\frac{3}{10}i\varepsilon \tag{75}$$

$$I_4=\int_0^{\pi/2}\cos^2\theta\,(\sin\theta)^{2i\varepsilon}\,d\theta\approx\frac{1}{\cosh(\pi\varepsilon)}\left(\frac{\pi}{4}-\frac{19}{10}i\varepsilon\right) \tag{76}$$

The stress intensity factors can be related to the energy release rates through the matrix $\widetilde{\boldsymbol{A}}$;

$$\widetilde{A}_{iklj}=\sum_{n=1}^{3}\sum_{m=1}^{3}\xi_{n+3(m+1)}U_{ki}^{(m)}V_{lj}^{(n)} \tag{77}$$

where

$$
\begin{aligned}
\xi_1 &= \frac{1}{2\pi\Delta}\int_0^{\Delta}\sqrt{\frac{\Delta-r}{r}}dr = \frac{1}{4} \\
\xi_2 &= \frac{1}{2\pi\Delta}\int_0^{\Delta}\sin(\varepsilon\ln r)\sqrt{\frac{\Delta-r}{r}}dr \\
&= \frac{1}{\pi}[\cos(\varepsilon\ln\Delta)\,\mathrm{Im}I_4 + \sin(\varepsilon\ln\Delta)\,\mathrm{Re}I_4] \\
\xi_3 &= \frac{1}{2\pi\Delta}\int_0^{\Delta}\cos(\varepsilon\ln r)\sqrt{\frac{\Delta-r}{r}}dr \\
&= \frac{1}{\pi}[\cos(\varepsilon\ln\Delta)\,\mathrm{Re}I_4 - \sin(\varepsilon\ln\Delta)\,\mathrm{Im}I_4] \\
\xi_4 &= \frac{1}{2\pi\Delta}\int_0^{\Delta}\sin(\varepsilon\ln(\Delta-r))\sqrt{\frac{\Delta-r}{r}}dr \\
&= \frac{1}{\pi}[\cos(\varepsilon\ln\Delta)\,\mathrm{Im}I_3 + \sin(\varepsilon\ln\Delta)\,\mathrm{Re}I_3] \\
\xi_5 &= \frac{1}{2\pi\Delta}\int_0^{\Delta}\sin(\varepsilon\ln r)\sin(\varepsilon\ln(\Delta-r))\sqrt{\frac{\Delta-r}{r}}dr \\
&= \frac{1}{2\pi}[-\cos(2\varepsilon\ln\Delta)\,\mathrm{Re}I_1 + \sin(2\varepsilon\ln\Delta)\,\mathrm{Im}I_1 + \mathrm{Re}I_2] \\
\xi_6 &= \frac{1}{2\pi\Delta}\int_0^{\Delta}\cos(\varepsilon\ln r)\sin(\varepsilon\ln(\Delta-r))\sqrt{\frac{\Delta-r}{r}}dr \\
&= \frac{1}{2\pi}[\cos(2\varepsilon\ln\Delta)\,\mathrm{Im}I_1 + \sin(2\varepsilon\ln\Delta)\,\mathrm{Re}I_1 + \mathrm{Im}I_2] \\
\xi_7 &= \frac{1}{2\pi\Delta}\int_0^{\Delta}\cos(\varepsilon\ln(\Delta-r))\sqrt{\frac{\Delta-r}{r}}dr \\
&= \frac{1}{\pi}[\cos(\varepsilon\ln\Delta)\,\mathrm{Re}I_3 - \sin(\varepsilon\ln\Delta)\,\mathrm{Im}I_3] \\
\xi_8 &= \frac{1}{2\pi\Delta}\int_0^{\Delta}\sin(\varepsilon\ln r)\cos(\varepsilon\ln(\Delta-r))\sqrt{\frac{\Delta-r}{r}}dr \\
&= \frac{1}{2\pi}[\cos(2\varepsilon\ln\Delta)\,\mathrm{Im}I_1 + \sin(2\varepsilon\ln\Delta)\,\mathrm{Re}I_1 - \mathrm{Im}I_2] \\
\xi_9 &= \frac{1}{2\pi\Delta}\int_0^{\Delta}\cos(\varepsilon\ln r)\cos(\varepsilon\ln(\Delta-r))\sqrt{\frac{\Delta-r}{r}}dr \\
&= \frac{1}{2\pi}[\cos(2\varepsilon\ln\Delta)\,\mathrm{Re}I_1 - \sin(2\varepsilon\ln\Delta)\,\mathrm{Im}I_1 + \mathrm{Re}I_2]
\end{aligned}
\tag{78}
$$

The matrix $\widetilde{\boldsymbol{B}}$ which relates the stress intensity factors k with the energy release rates $\widetilde{\boldsymbol{g}}$ using the matrix $\widetilde{\boldsymbol{A}}$.

$$\widetilde{\boldsymbol{B}}\,\widetilde{\boldsymbol{k}} = \widetilde{\boldsymbol{g}} \tag{79}$$

where

$$\widetilde{\boldsymbol{k}} = \{K_I^2, K_{II}^2, K_{III}^2, K_{II}K_{III}, K_IK_{III}, K_IK_{II}\} \tag{80}$$

$$\widetilde{\boldsymbol{g}} = \{G_I, G_{II}, G_{III}, G_{II-III}, G_{I-III}, G_{I-II}\} \tag{81}$$

$$\widetilde{\boldsymbol{B}} = \begin{bmatrix} \alpha_{2222} & \alpha_{1221} & \alpha_{3232} \\ \alpha_{2112} & \alpha_{1111} & \alpha_{3113} \\ \alpha_{2332} & \alpha_{1331} & \alpha_{3333} \\ \alpha_{2132}+\alpha_{2312} & \alpha_{1131}+\alpha_{1311} & \alpha_{3133}+\alpha_{3313} \\ \alpha_{2232}+\alpha_{2322} & \alpha_{1231}+\alpha_{1321} & \alpha_{3233}+\alpha_{3323} \\ \alpha_{2122}+\alpha_{2212} & \alpha_{1121}+\alpha_{1211} & \alpha_{3123}+\alpha_{3213} \end{bmatrix} \tag{82}$$

$$\begin{bmatrix} \alpha_{1223}+\alpha_{3221} & \alpha_{2223}+\alpha_{3222} \\ \alpha_{1113}+\alpha_{3111} & \alpha_{2113}+\alpha_{3112} \\ \alpha_{1333}+\alpha_{3331} & \alpha_{2333}+\alpha_{3332} \\ \alpha_{1133}+\alpha_{3131}+\alpha_{1313}+\alpha_{3311} & \alpha_{2133}+\alpha_{3132}+\alpha_{2313}+\alpha_{3312} \\ \alpha_{1233}+\alpha_{3231}+\alpha_{1323}+\alpha_{3321} & \alpha_{2132}+\alpha_{2312}+\alpha_{2132}+\alpha_{2312} \\ \alpha_{1123}+\alpha_{3121}+\alpha_{1213}+\alpha_{3211} & \alpha_{2123}+\alpha_{3122}+\alpha_{2213}+\alpha_{3212} \end{bmatrix}$$

$$\begin{bmatrix} \alpha_{1222}+\alpha_{2221} \\ \alpha_{1112}+\alpha_{2111} \\ \alpha_{1332}+\alpha_{2331} \\ \alpha_{1132}+\alpha_{2131}+\alpha_{1312}+\alpha_{2311} \\ \alpha_{1232}+\alpha_{2231}+\alpha_{1322}+\alpha_{2321} \\ \alpha_{1122}+\alpha_{2121}+\alpha_{1212}+\alpha_{2211} \end{bmatrix} \tag{83}$$

The square of the stress intensity factors, K_I^2 , K_{II}^2 and K_{III}^2, can be easily solved from the linear equation in Eq.79. The signs for the stress intensity factors, K_I , K_{II} and K_{III}, can be ascertained from the crack opening displacements.

3.5 Numerical examples

Symmetric laminates under tensile loading

Consider a symmetric laminate under uniaxial tension as shown in Fig. 8. The edge delamination crack front is assumed to be parallel to the x_3 axis and growing in the x_2 direction along the interface between two dissimilar laminae. Therefore, only the cross section along the specimen width is modeled using the quasi three-dimensional finite element method. For a generalized plane strain condition, the displacement of the "Quasi 3-D" deformation has the form of

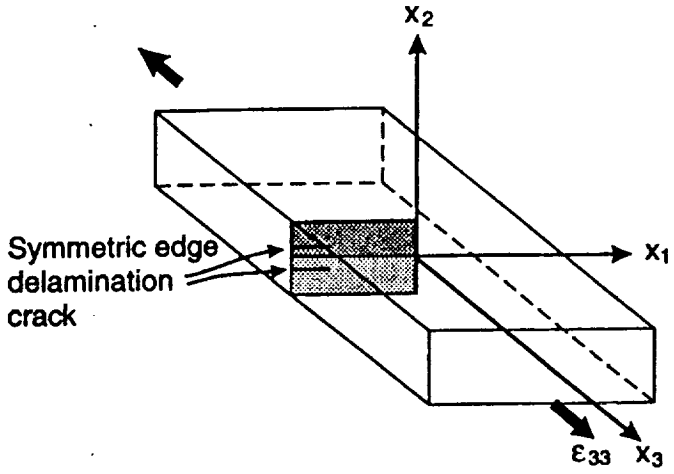

Figure 8: Schematic of edge delamination cracks in a symmetric laminate under uniaxial strain

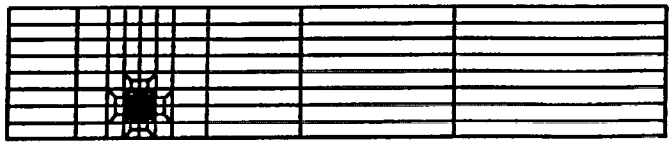

Figure 9: The mesh for $[\pm 45/0/90]_s$ and $[0/\pm 45/90]_s$ laminate with an edge delamination crack between the 0 and 90 degree ply

$$\begin{aligned} u_1 &= U_1(x_1,x_2) \\ u_2 &= U_2(x_1,x_2) \\ u3 &= U_3(x_1,x_2)+\varepsilon_{33}x_3 \end{aligned} \tag{84}$$

Due to the symmetry conditions of the laminate and the uniaxial load, only a quarter of the cross section needs to be modeled (with the mesh shown in Fig. 9).

Two different laminates (made of T300-5208 carbon epoxy) are considered in the present study; $[0/\pm 45/90]_S$ and $[\pm 45/0/90]_S$. The onset of delamination crack propagation in both laminates can be attributed to the mismatch in the lateral contraction (due to the Poisson's effect) between the 90 plies and plies of different angles. The computed stress intensity factors with the ply thickness as the characteristic length are tabulated in Tab. 5. This result using the virtual crack closure method compares favorably with the result by Chow et al. (1995) using the mutual integral method with the particular solution. The difference between these two solutions is less than 2%.

Table 5: Stress Intensity Factors for a delamination crack in a laminate under uniaxial tension

Laminate	Crack between	Virtual Crack Closure Integral Method			Interactive Integral with Particular Solution		
		$\frac{\varepsilon_{33}\hat{K}_I}{K_{IC}}$	$\frac{\varepsilon_{33}\hat{K}_{II}}{K_{IIC}}$	$\frac{\varepsilon_{33}\hat{K}_{III}}{K_{IIIC}}$	$\frac{\varepsilon_{33}\hat{K}_I}{K_{IC}}$	$\frac{\varepsilon_{33}\hat{K}_{II}}{K_{IIC}}$	$\frac{\varepsilon_{33}\hat{K}_{III}}{K_{IIIC}}$
$[\pm 45/0/90]_S$	0/90	145.9	29.0	-1.4	145.2	29.5	-1.4
$[0/\pm 45/90]_S$	$-45/90$	80.4	64.9	-6.9	79.5	65.6	-7.0

Characteristic length = t_{ply}

K_{IC} = 0.88 MPa$\sqrt{m}$, K_{IIC} = 2.9 MPa$\sqrt{m}$, and K_{IIIC} = 2.3 MPa$\sqrt{m}$.

BIBLIOGRAPHY

Beom, H. G.; Atluri, S. N. (1994): *Near-tip fields and stress intensity factors for interfacial cracks in dissimilar anisotropic media.* Center for Computational Mechanics, Georgia Institute of Technology, March.

Cho, Y. J.; Beom, H. G.; Earmme, Y. Y. (1994): Application of a conservation integral to an interface crack interaction with singularities. *Int. J. Frac.*, v.65, pp.63-73.

Chow, W. T.; Atluri, S. N. (1995): Finite element calculation of stress intensity factors for interfacial crack using virtual crack closure integral. *Comput. Mech.*, v.16, pp.417-425.

Chow, W. T.; Atluri, S. N. (1996): Stress intensity factors as the fracture parameters for delamination crack growth in thick composite laminates. *Comput. Mech.*, (to appear).

Chow, W. T.; Beom, H. G.; Atluri, S. N. (1995): Calculation of stress intensity factors for an interfacial crack between dissimilar anisotropic media, using a hybrid element method and the mutual integral. *Comput. Mech.*, v.15, pp.546-557.

Dundurs, J. (1969): Discussion of "edge-bonded dissimilar orthogonal elastic wedges under normal and shear loading". *J. Appl. Mech. Trans. ASME*, v.36, pp.650-652.

Herakovich, C. T. (1982): Influence of layer thickness on the strength of angle-ply. .

Irwin, G. R. (1958): Fracture. *Handbook der Physik*, v.6, pp.551.

Kathiresan, K.; Atluri, S. N. (1978): Homogeneous and bimaterial crack elements for analysis of solid rocket motor grains. *v.I AFRPL-TR-78-286*, pp. 200, Edwards Airforce Base, CA.

Lin, K. Y.; Mar, J. W. (1976): Finite element analysis of stress intensity factors for cracks at a bi-material interface. *Int. J. Frac.*, v.12, pp.521-531.

Lucas, J. P. (1992): Delamination fracture effect of fiber orientation on fracture of a continuous fiber composite laminate. *Eng. Frac. Mech.*, v.42, pp.543-561.

O'Brien, T. K. (1982): Characterization of delamination onset and growth in composite laminate. *Damage in Composite Materials*, ASTM STP 775, pp. 140-167.

Qu, J.; Bassani, J. L. (1993): Interfacial fracture mechanics for anisotropic bimaterials. *J. Appl. Mech. Trans. ASME*, v.,, pp.60422-431.

Qu, J.; Li, Q. (1991): Interfacial dislocation and its application to interface cracks in anisotropic bimaterials. *J. Elasticity*, v.26, pp.169-195.

Raju, I. S. (1987): Calculation of strain-energy release rates with higher order and singular finite elements. *Eng. Frac. Mech.*, v.28, pp.251-274.

Raju, I. S.; Crews, J. H. J.; Aminpour, M. A. (1988): Convergence of strain energy release rate components for edge-delaminated composite laminates. *Eng. Frac. Mech.*, v.30, pp.383-396.

Rice, J. R. (1988): Elastic fracture mechanics concepts for interfacial cracks. *J. Appl. Mech. Trans. ASME*, v.55, pp.98-103.

Rice, J. R.; Sih, G. C. (1965): Plane problems of cracks in dissimilar media. *J. Appl. Mech. Trans. ASME*, v.32, pp.403-410.

Rybicki, E. F.; Kanninen, M. F. (1977): A finite element calculation of stress intensity factors by a modified crack closure integral. *Eng. Frac. Mech.*, v.9, pp.931-938.

Sendeckyi, G. P.; Richardson, M. D.; Pappas, J. E. (1975): Fracture behavior of thornel 300/5208 graphite-epoxy laminates-part 1 unnotched laminates. *Composite Reliability, ASTM STP 580*, pp. 528-546.

Shanbhag, M. R.; Eswaran, K.; Maiti, S. K. (1993): Measurement of fracture toughness of bimaterial interfaces and a stress-based approach to their fracture. *Eng. Frac. Mech.*, v.44, pp.75-89.

Sun, C. T.; Jih, C. J. (1987): On strain energy release rate for interfacial cracks in bimaterial media. *Eng. Frac. Mech.*, v.28, pp.13-20.

Wang, J. S.; Suo, Z. (1990): Experimental determination of interfacial toughness using Brazil-nut-sandwich. *Acta Met.*, v.38, pp.1279-1290.

Williams, M. L. (1959): The stresses around a fault or crack in dissimilar media. *Bull. Seismol. Soc. America*, v.49, pp.199-204.

Wu, K. C. (1989): Representations of stress intensity fators by path-indepenedent integrals. *J. Appl. Mech. Trans. ASME*, v.56, pp.780-785.

Yuuki, R.; Liu, J. Q.; Xu, J. Q.; Ohira, T.; Ono, T. (1994): Mixed mode fracture criteria for an interface crack. *Eng. Frac. Mech.*, v.47, pp.367-377.